PERGAMON

International Journal of Solids and Structures 38 (2001) 8155–8169

INTERNATIONAL JOURNAL OF SOLIDS and STRUCTURES

www.elsevier.com/locate/ijsolstr

Land surface uplift above compacting overconsolidated reservoirs

Massimiliano Ferronato *, Giuseppe Gambolati, Pietro Teatini, Domenico Baù

Department of Mathematical Methods and Models for Scientific Applications (DMMMSA), University of Padova, Via Belzoni 7, 35131 Padova, Italy

Received 7 March 2001; in revised form 7 May 2001

Abstract

An investigation on land surface deformation resulting from the compaction of producing overconsolidated gas/oil reservoirs is presented. If the depleted formation is significantly less compressible than the surrounding medium the vertical reservoir shrinkage is relatively smaller than the horizontal one, thus generating a possible swelling of the overburden and a consequent pronounced decrease of land subsidence or even a surface uplift. Such an effect may also cause an additional land settlement during the post-productive recovery phase over fields which exhibit a stiffer behavior in expansion. In the present paper the surface displacements caused by the depletion of an overconsolidated disk-shaped reservoir are analyzed by a finite element model taking into account the influence of the disk burial depth and areal extent, the Poisson ratio of the medium, and the underburden stiffness. The results obtained with a more realistic three-dimensional setting are also discussed to address the possible effects of an irregular reservoir geometry.

Keywords: Land subsidence; Finite elements; Reservoir compaction; Compressibility contrast

1. Introduction

It is well-known that the production of oil and natural gas from underground reservoirs causes a pore pressure decrease within the depleted formations which induces a compaction of the developed unit. The major consequence is anthropogenic land subsidence, as has been widely experienced in many areas during the last decades. Examples of subsidence above compacting gas/oil fields may be found in Long Beach, California (Colazas and Strehle, 1995), in Venezuela (Finol and Sancevic, 1995), and in the North Sea Ekofisk field (Zaman et al., 1995). The coastal area of the Northern Adriatic Sea, Italy, is a recent example of possible land subsidence due to gas pumping (Gambolati et al., 1991, 1998; Teatini et al., 1998, 2000; Palozzo et al., 2000).

* Corresponding author. Tel.: +39-049-827-5929; fax: +39-049-827-5995.
E-mail address: ferronat@dmsa.unipd.it (M. Ferronato).

0020-7683/01/$ - see front matter
PII: S0020-7683(01)00122-6

The stress–strain relations of permeable fluid-saturated materials have been discussed by Biot (1941) using a consolidation theory that couples the porous medium stress and flow fields. The analytical solution to land subsidence over a disk-shaped reservoir embedded in a homogeneous elastic half space was contributed by Geertsma (1966, 1973a). Recently an original derivation of the solution for a reservoir of arbitrary shape has been developed by Verruijt (2000) using the approximate method by Sagaseta (1987) for an incompressible material. In realistic field situations a reliable prediction of land subsidence requires an ad hoc appropriate numerical model able to address a number of issues, such as three-dimensional (3-D) geometry, medium heterogeneity, layering, coupling, elasto-plasticity, etc. Nevertheless, simplified elastic solutions may still be of a great help in giving a rough and almost inexpensive estimate of the expected impact that gas/oil withdrawal can exert on land stability.

Geertsma's (1973a) theoretical solution can usually be quite acceptable when the depletion of the aquifer surrounding a gas/oil reservoir is negligible (Baù et al., 2001). However, in a few examples an unexpected behavior may be observed. Some fields may compact during production with apparently no ground settlement, as is the case of the Crotone area in Calabria, Italy (Bertoni et al., 2000), or additional land subsidence may still take place even though the gas/oil bearing formation is expanding, because of the influence of an active waterdrive (Baù et al., 1999) or an external fluid injection (Hermansen et al., 2000). In particular, in the above examples the assumption of mechanical medium homogeneity, as is typically made with analytical simplified formulations, is not acceptable, since the effective stress change may increase significantly the reservoir stiffness, thus generating an overconsolidation state.

The present paper addresses the calculation of land surface settlement due to the compaction of an overconsolidated reservoir embedded in a homogeneous elastic half space using a finite element (FE) numerical model solved with the aid of the infinite pore pressure gradient approach (Gambolati et al., 2001). The purpose is to give an indication as to the surface deformation when significant compressibility contrasts exist between the gas/oil bearing formations and the surrounding medium. It is shown that unexpected results may be obtained, with a compacting reservoir and nevertheless no land subsidence, as is sometimes observed in real world problems, or even an uplift for reservoirs much stiffer than the remainder of the porous medium.

The paper is organized as follows. The mathematical model is briefly reviewed and validated against well-known analytical solutions. The land settlement above a spherical and a cylindrical depleted reservoir is compared, and the possible inception of uplift phenomena shown. In the cylindrical problem the stress–strain field is studied taking into account the influence of the burial depth h, the reservoir radius R, and the Poisson ratio v on land surface deformation for various ratios between the compressibilities of the overconsolidated reservoir and the remaining medium. A 3-D problem is solved to investigate how the field geometry may affect the results obtained with the ideal disk-shaped reservoir. The case of an underburden stiffer than the overburden is also addressed. Finally, a set of concluding remarks is issued.

2. Infinite pore pressure gradient approach

The problem addressed herein concerns an elastic half space bounded by an upper traction free surface. The loading is due to a pore pressure decline occurring within a finite reservoir embedded in the elastic continuum. Zero displacements are theoretically set at infinity, practically at a sufficiently large distance from the depleted volume. We deal with an initial equilibrium configuration, so all the variables related to stress, strain, and displacements are expressed in terms of incremental quantities, which are independent on the in situ stress. A schematic representation of the physical problem and its boundary conditions is shown in Fig. 1.

Since the system is in equilibrium at the global level, the virtual work principle applies to the whole medium:

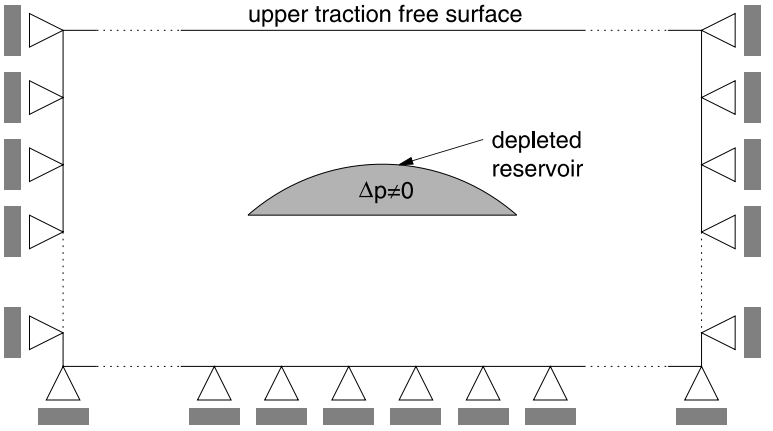

Fig. 1. Schematic vertical cross-section of the elastic half space embedding a finite producing reservoir.

$$\int_V \boldsymbol{\epsilon}^{\mathrm{T}}\boldsymbol{\sigma}\,\mathrm{d}V = \int_V \boldsymbol{u}^{\mathrm{T}}\boldsymbol{q}^{\mathrm{ex}}\,\mathrm{d}V \tag{1}$$

with $\boldsymbol{\sigma}$ and $\boldsymbol{\epsilon}$ the stress and strain vectors, respectively, $\boldsymbol{u}$ the displacements, $\boldsymbol{q}^{\mathrm{ex}}$ the distributed external source of strength and V the porous medium volume. Using the classical FE approach for the elastic continuum equilibrium (Zienkiewicz and Taylor, 1989) yields:

$$\boldsymbol{\epsilon} = \boldsymbol{L}\boldsymbol{u} = \boldsymbol{L}\boldsymbol{N}\boldsymbol{\delta} = \boldsymbol{B}\boldsymbol{\delta} \tag{2}$$

where $\boldsymbol{L}$ is an appropriate differential operator, $\boldsymbol{N}$ the shape function matrix, and $\boldsymbol{\delta}$ the displacement component vector. Substituting Eq. (2) into Eq. (1) and canceling the virtual displacement $\boldsymbol{\delta}$ give the standard FE equilibrium equation:

$$\int_V \boldsymbol{B}^{\mathrm{T}}\boldsymbol{\sigma}\,\mathrm{d}V + \boldsymbol{f}^{\mathrm{ex}} = 0 \tag{3}$$

with $\boldsymbol{f}^{\mathrm{ex}}$ the external strength term equal to $-\int_V \boldsymbol{N}^{\mathrm{T}}\boldsymbol{q}^{\mathrm{ex}}\,\mathrm{d}V$.

If the porous medium is fully saturated, the following relation holds for the stress vector (Biot, 1941; Terzaghi and Peck, 1967):

$$\boldsymbol{\sigma} = \boldsymbol{\sigma}_{\mathrm{eff}} - \alpha\boldsymbol{i}p \tag{4}$$

where α is the Biot coefficient, $\boldsymbol{i}$ the Kronecker δ in vectorial form and p the pore pressure. The rock matrix deformation is related to the effective intergranular stress $\boldsymbol{\sigma}_{\mathrm{eff}}$ exclusively.

Since the only stress source is the pore pressure change, $\boldsymbol{f}^{\mathrm{ex}} = 0$ and replacing Eq. (4) into Eq. (3) leads to:

$$\int_V \boldsymbol{B}^{\mathrm{T}}\boldsymbol{\sigma}_{\mathrm{eff}}\,\mathrm{d}V = \int_V \alpha\boldsymbol{B}^{\mathrm{T}}\boldsymbol{i}p\,\mathrm{d}V = \boldsymbol{f} \tag{5}$$

As 3-D tetrahedral elements are used, so the pore pressure p is linear over each finite element. Vector $\boldsymbol{f}$ of Eq. (5) can be expressed as (Gambolati et al., 2001):

$$\boldsymbol{f} = \sum_e \int_{V_e} \alpha\boldsymbol{B}^{\mathrm{T}}\boldsymbol{i}p\,\mathrm{d}V_e = \sum_e \left(\alpha\boldsymbol{B}^{\mathrm{T}}\boldsymbol{i}\right)_e \int_{V_e} p\,\mathrm{d}V_e = \sum_e (\alpha\boldsymbol{B}^{\mathrm{T}}\boldsymbol{i}V\bar{p})_e \tag{6}$$

where the symbols with pedix e are referred to a generic finite element, $\bar{p}$ is the average elemental value of p, and $\sum_e$ stands for the assemblage operation. Eq. (6) allows for the FE solution to the problem of a finite

reservoir subject to a pore pressure decline with an abrupt drop to zero (i.e. an infinite pore pressure gradient) on its boundary (Gambolati et al., 2001), as is usually assumed in idealized reservoir representations (Geertsma, 1973a,b; Geertsma and van Opstal, 1973).

2.1. Model validation over a spherical reservoir

The FE model described above is used to predict the surface settlement induced by the depletion of a finite reservoir with different mechanical properties than the remaining medium. An analytical solution to this problem may be found in Gambolati (1972) for a spherical reservoir. Land subsidence $\eta = \eta_{\text{cen}}$ over the center of the sphere reads:

$$\eta_{\text{cen}} = -\frac{1-v^2}{\pi E_{\text{m}}} \cdot \Delta p \cdot \frac{c_{\text{R,v}}}{\frac{2}{3} c_{\text{R,v}} + \frac{1+v}{E_{\text{m}}}} \cdot \frac{V_{\text{s}}}{h^2} \tag{7}$$

where h is the sphere burial depth, V_{s} the depleted volume, v the Poisson ratio assumed to be the same outside and inside the sphere, E_{m} the Young modulus of the medium embedding the reservoir, $c_{\text{R,v}}$ the reservoir volumetric compressibility, and Δp the pressure decline.

If the spherical nucleus is homogeneous with the rest of the medium, then $c_{\text{R,v}}$ is equal to the compressibility $c_{\text{m,v}} = 3(1-2v)/E_{\text{m}}$ and Eq. (7) gives Geertsma's (1966) solution:

$$\eta_{\text{hom}} = -\frac{1-v^2}{\pi E_{\text{m}}} \cdot \Delta p \cdot \frac{3(1-2v)}{E_{\text{m}}} \cdot \frac{E_{\text{m}}}{2(1-2v)+1+v} \cdot \frac{V_{\text{s}}}{h^2} = -\frac{(1+v)(1-2v)}{\pi E_{\text{m}}} \cdot \Delta p \cdot \frac{V_{\text{s}}}{h^2}$$

The dimensionless ratio between η_{cen} and η_{hom} is:

$$H = \frac{\eta_{\text{cen}}}{\eta_{\text{hom}}} = \frac{1-v}{1-2v} \cdot \frac{c_{\text{R,v}}}{\frac{2}{3} c_{\text{R,v}} + \frac{1+v}{E_{\text{m}}}} \tag{8}$$

Setting $C = \frac{c_{\text{R,v}}}{c_{\text{m,v}}}$ and remembering the $c_{\text{m,v}}$ expression, Eq. (8) becomes:

$$H = \frac{\eta_{\text{cen}}}{\eta_{\text{hom}}} = \frac{1-v}{1-2v} \cdot \frac{C c_{\text{m,v}}}{\frac{2}{3} C c_{\text{m,v}} + \frac{(1+v)c_{\text{m,v}}}{3(1-2v)}} = \frac{3C(1-v)}{2C(1-2v)+1+v} \tag{9}$$

Eq. (9) shows that H is a nonlinear function of C, for any $v \neq 0.50$, and v. Since v is taken to be the same for the reservoir and the surrounding medium, C is also equal to $c_{\text{R}}/c_{\text{m}}$, c_{R} and c_{m} being the vertical (oedometric) reservoir and medium compressibility, respectively.

The FE model is validated by comparison with the analytical solution (9) for $0 < C \leqslant 1$, i.e. an overconsolidated spherical nucleus stiffer than the embedding medium. A 3000 m deep sphere with a 20 m diameter is simulated. Standard Dirichlet conditions with zero radial displacements on the symmetry axis and fixed bottom and outer boundaries, 10 000 m deep and 15 000 m far, respectively, are prescribed. The medium compressibility $c_{\text{m,v}}$ is 10^{-4} cm^2/kg, with $c_{\text{R,v}} = C \cdot c_{\text{m,v}}$, and a uniform unit pore pressure decline is taken within the sphere. The analytical and the numerical solutions are shown in Fig. 2 for different Poisson ratios.

Note that the FE model provides a very accurate solution. As expected, land subsidence over the sphere center is not linear with $c_{\text{R,v}}$, and H is always larger than C, with the difference becoming smaller for $c_{\text{R,v}} \to 0$ and $c_{\text{R,v}} \to c_{\text{m,v}}$.

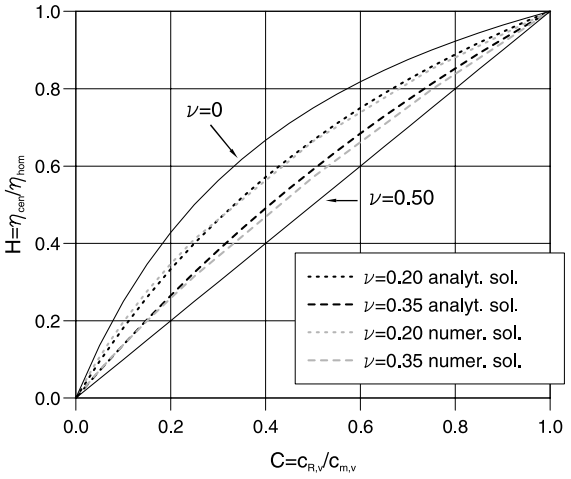

Fig. 2. Ratio η_{cen}/η_{hom} vs C and different v values for an overconsolidated spherical reservoir ($C \leqslant 1$) as provided by the analytical (Eq. (9)) and the numerical models. Solid profiles with v equal to 0 and 0.5 are obtained by the analytical solution.

3. Influence of C for a cylindrical reservoir

We investigate the influence of the field shape on the results shown in Fig. 2 by transforming the overconsolidated spherical reservoir into a disk-shaped one with constant thickness s, equal to the sphere diameter, i.e. 20 m, and a growing radius R. This is simply obtained from the previous numerical model by prescribing a unit pressure decline and a different compressibility over an increasing number of adjacent finite elements (Fig. 3a). The ratio H vs C is given in Fig. 3b, where the results for the spherical reservoir are also provided. It may be noted that the profile concavity changes, and a zero or reverse subsidence may occur on the symmetry axis for $C < 0.4$ (and $R = 100$ m, $v = 0.35$). A reverse subsidence means a land

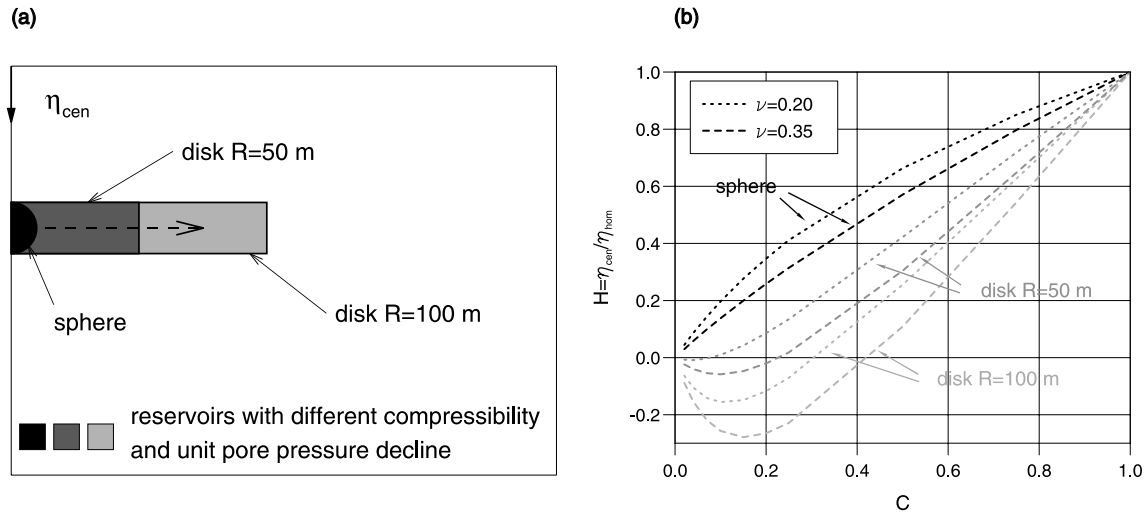

Fig. 3. (a) Schematic representation of the reservoir transformation from a spherical into a disk-shaped one; compressibility c_R and unit pore pressure decline apply in the gray shaded areas; (b) ratio η_{cen}/η_{hom} vs C for different reservoir radii R and Poisson ratios v.

surface uplift over a compacting reservoir, or symmetrically an additional settlement over an expanding reservoir, which turn out to be more pronounced for larger v and R. Therefore land surface above a producing cylindrical reservoir may rise depending on C, i.e. the overconsolidation degree, for suitably large value of Poisson ratio and outer radius. This result appears to be quite surprising, and to our knowledge has never been pointed out before.

3.1. Stress–strain analysis

Let us consider the stress–strain field generated by the depletion of a cylindrical reservoir 3000 m deep, 20 m thick, with $R = 1000$ m and $v = 0.25$. We assume that the field belongs to an overconsolidated layer with vertical compressibility $c_R = C \cdot c_m$, $0 < C \leqslant 1$ and $c_m = 10^{-4}$ cm^2/kg. A unit pore pressure decline is prescribed within the reservoir with the boundary conditions described in the previous section. Note that the results discussed below hold true with opposite sign if a depleted reservoir experiences a unit pore pressure recovery. The FE mesh totaling 7905 nodes and 15 450 elements is shown in Fig. 4. The ratio between land subsidence η and the homogeneous half-space subsidence η_{Geer} (Geertsma, 1973a):

$$\eta_{Geer} = -2(1-v)c_m s\,\Delta p\left[1 - \frac{h/R}{\sqrt{1+(h/R)^2}}\right] \tag{10}$$

is plotted vs the radial distance r in Fig. 5 for various $C \leqslant 1$. This figure reveals that at $r = 0$, η/η_{Geer} decreases proportionally more than C does, and for $C \simeq 0.5$ the land settlement over the center of the field vanishes. Also note that the location experiencing the maximum subsidence no longer lies on the symmetry axis. For $C < 0.5$ the surface above the compacting formation exhibits an uplift which achieves its largest

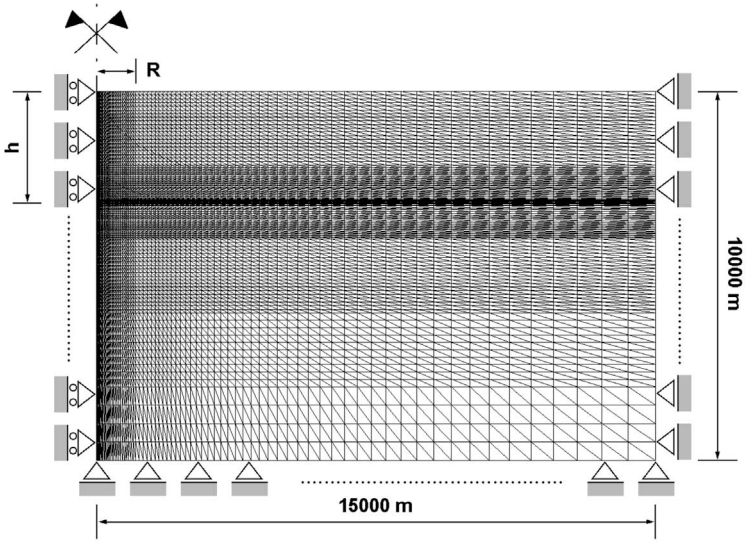

Fig. 4. Finite element mesh used in the axisymmetric reservoir problems.

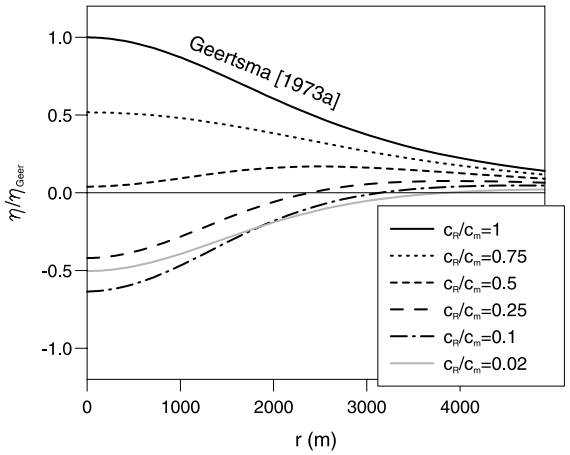

Fig. 5. Land subsidence η relative to η_{Geer} (Eq. (10)) vs distance r from the symmetry axis for different C ratios in the case of depletion of a reservoir 3000 m deep, 20 m thick, with $R = 1000$ m.

relative value for $C = 0.1$. For decreasing C, η gradually approaches zero, as is theoretically expected. Thus, the profiles for small C values (e.g. $C = 0.02$) may intersect those related to $C = 0.1$. It is worth emphasizing that the maximum predicted uplift for $C = 0.1$ is about 60% of the land subsidence occurring over the center of the field in the homogeneous porous medium (Eq. (10)).

A useful parameter to estimate the impact that gas/oil withdrawal may exert on the stability of the ground surface is the land subsidence spreading factor $\chi = \eta/\xi$ (Baù et al., 2001), where ξ is the vertical reservoir compaction. The $\chi_{cen} = \eta_{cen}/\xi_{cen}$ values calculated at $r = 0$ are shown vs C in Fig. 6b, while Fig. 6a shows the corresponding η_{cen} and ξ_{cen} normalized with the reservoir oedometric compaction $c_m s\Delta p$ of the

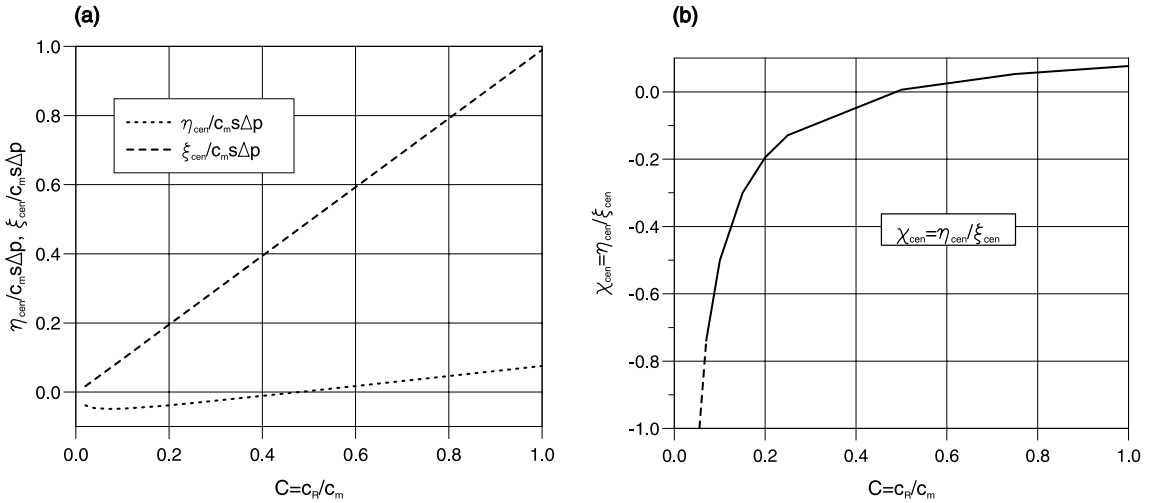

Fig. 6. (a) Surface settlement η_{cen} and reservoir compaction ξ_{cen} normalized against $c_m s\Delta p$; (b) land subsidence spreading factor χ_{cen} vs C at $r = 0$.

homogeneous case. Observe that the reservoir vertical compaction on the symmetry axis is always equal to $c_R s \Delta p$, as it would occur under oedometric conditions (dashed profile of Fig. 6a). By distinction, the transference of reservoir compaction to ground surface is strongly influenced by the compressibility contrast. In fact, the spreading factor χ_{cen} is equal to Geertsma's (1973a) theoretical value χ_{Geer}:

$$\chi_{Geer} = 2(1-\nu)\left[1 - \frac{h/R}{\sqrt{1+(h/R)^2}}\right]$$

which is 0.077 in this case, only if the rock is slightly overconsolidated ($0.8 \leqslant C < 1$). For $C \simeq 0.5$, χ_{cen} changes sign, i.e. a reverse subsidence occurs, and increases for $C \to 0$ (Fig. 6b).

To help understand the results of Figs. 5 and 6 the principal stresses and the corresponding deformations are analyzed. The stress and strain fields are shown in Figs. 7–9 for three significant sample problems: $C = 1$ (homogeneous case), $C = 0.5$ (no land subsidence), and $C = 0.1$ (largest surface uplift). Fig. 7 shows the principal stresses σ_1 and σ_2:

$$\sigma_{1,2} = \frac{\sigma_{rr}+\sigma_{zz}}{2} \pm \frac{1}{2}\sqrt{(\sigma_{rr}-\sigma_{zz})^2 + 4\sigma_{rz}^2}$$
$$\vartheta = \frac{1}{2}\mathrm{arctg}\left(\frac{2\sigma_{rz}}{\sigma_{rr}-\sigma_{zz}}\right)$$

with ϑ denoting the angle that σ_1 and σ_2 form with the z and the r axis, respectively. Note that $\sigma_{rz} = 0$ near the symmetry axis, as expected, so σ_1 coincides with σ_{zz} and σ_2 with σ_{rr}. Also note that σ_1 decreases where the reservoir is stiffer (Fig. 7a, c, and e) with the occurrence of an area in the overburden with a stress of opposite sign, while σ_2 does not change significantly with C (Fig. 7b, d, and f). Fig. 7 points out the existence of a surface above the reservoir where an abrupt variation in the principal stress direction occurs.

The stress effects on porous medium deformation can be understood from Fig. 8 for the whole structure and from Fig. 9 for the zone surrounding the reservoir. The grids displayed in Figs. 8 and 9 are not the FE grids used for the calculation, which are much more refined (see Fig. 4). It can be noted that, as the gas/oil bearing formation becomes stiffer, the vertical compaction decreases, as can be also seen from Fig. 6, and the reservoir shrinks mainly in the horizontal direction. This result is pointed out by other authors as well (e.g. Bévillon et al. (2000)). The major consequence is a swelling of the overburden, which is consistent with the change of the σ_1 sign (see Fig. 7c and e), and a corresponding pronounced land subsidence decrease, or even a surface uplift. Also observe in Fig. 8 the rotation, as the reservoir becomes stiffer, of the surface over which the abrupt change in the principal stress direction occurs. This rotation emphasizes the arch effect which develops in the overburden.

3.2. Parametric analysis

The importance of uplift (or additional land subsidence, if the depleted reservoir is expanding) and the limiting C below which it occurs depend upon both the geometrical features of the reservoir (burial depth h and radius R) and the Poisson ratio ν, as can also be seen in Fig. 3b. A parametric study on the influence of h, R, and ν is performed to investigate more thoroughly the correlation between H and C.

Some significant results are given in Fig. 10. Fig. 10a shows that a larger Poisson ratio tends to emphasize the surface uplift. With $\nu = 0.35$ the reverse η_{cen} may exceed 80% the land subsidence predicted in the homogeneous case, while with a compressibility c_R slightly larger than half c_m ($C \simeq 0.55$) the

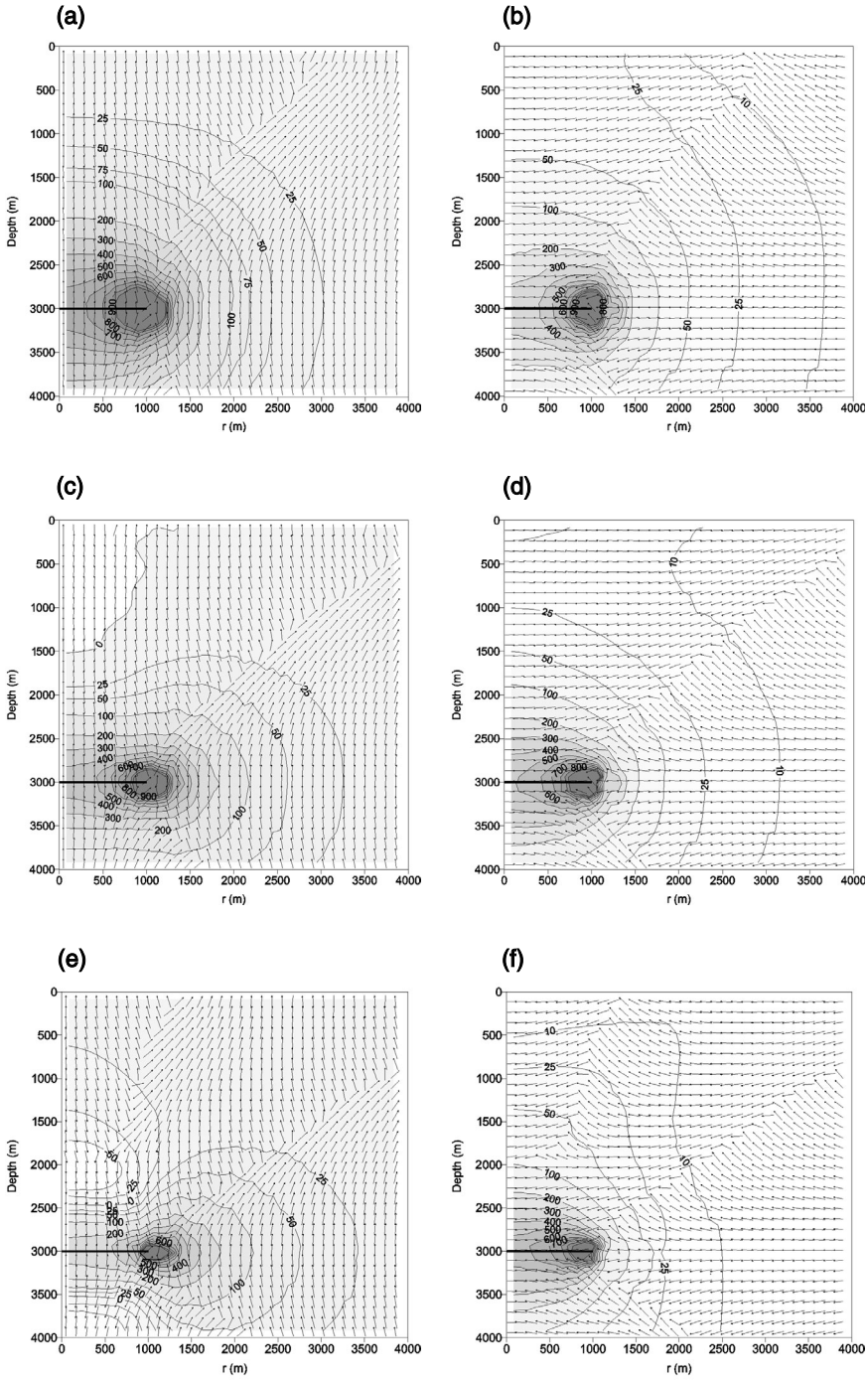

Fig. 7. Principal stress fields generated by the depletion of a disk-shaped reservoir 3000 m deep, 20 m thick, with $R = 1000$ m and $v = 0.25$: (a) σ_1 and (b) σ_2 for $C = 1$; (c) σ_1 and (d) σ_2 for $C = 0.5$; (e) σ_1 and (f) σ_2 for $C = 0.1$. Stress directions are represented by vectors, and the moduli by the shaded isolines. Numerical values are in kg/m^2.

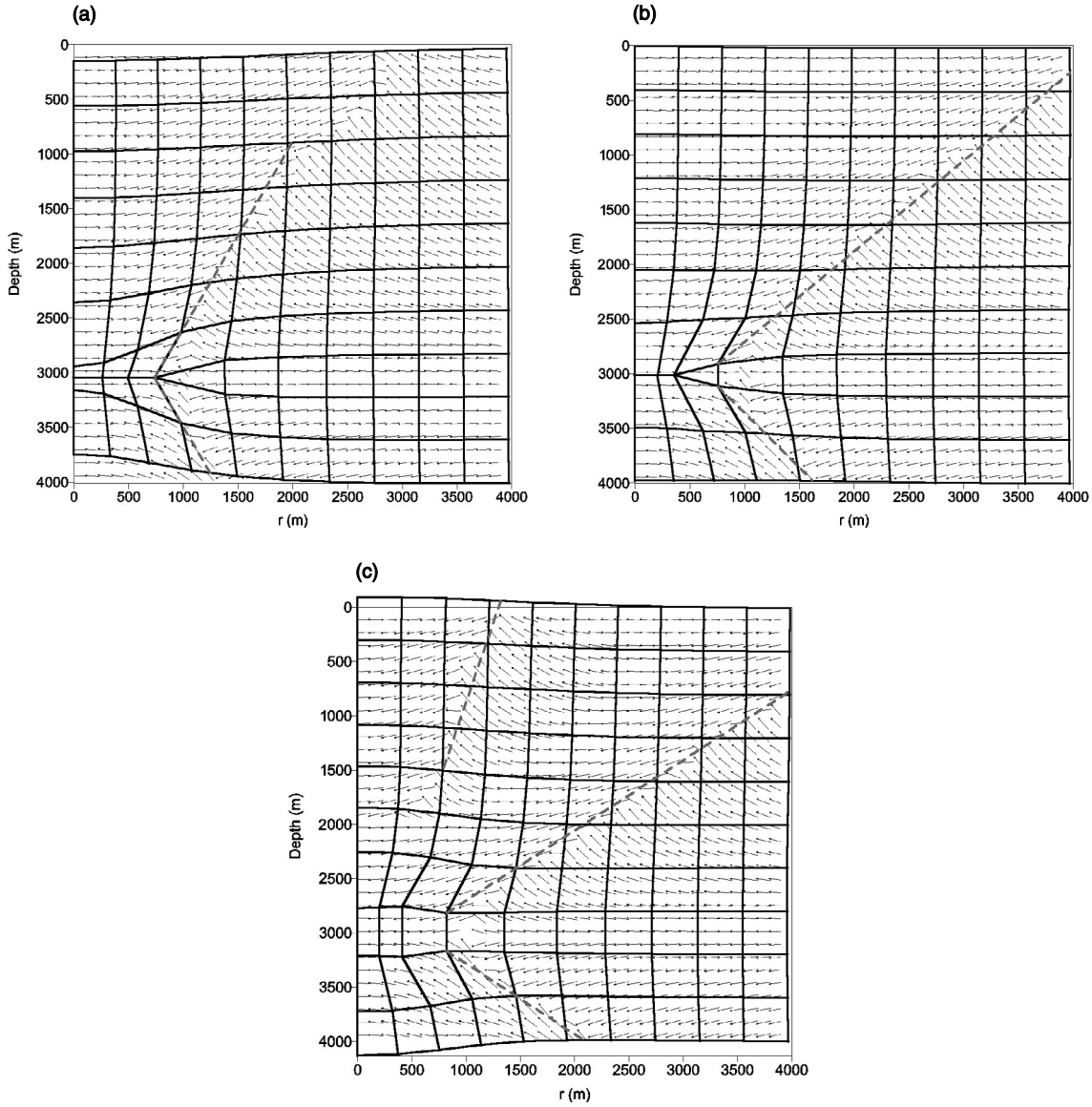

Fig. 8. Deformation of the porous medium due to reservoir depletion for: (a) $C = 1$; (b) $C = 0.5$; (c) $C = 0.1$. The exaggeration for horizontal and vertical displacements is 50 000. The vectors represent the σ_2 directions and the dashed lines the traces of the surfaces over which an abrupt change in the principal stress directions occurs.

settlement over the center of the field vanishes. Inspection of Fig. 10b and c also reveals that the uplift, or the additional subsidence, is more pronounced for deeper and relatively small ($R = 1000$ m) reservoirs. There is no simple relation between H and the ratio h/R. However, the present analysis seems to suggest that a larger h/R may produce a larger uplift. When the reservoir is shallower and areally extensive the deformation tends to become one-dimensional with $H \simeq C$ and no uplift (see the dashed profiles in Fig. 10b and c).

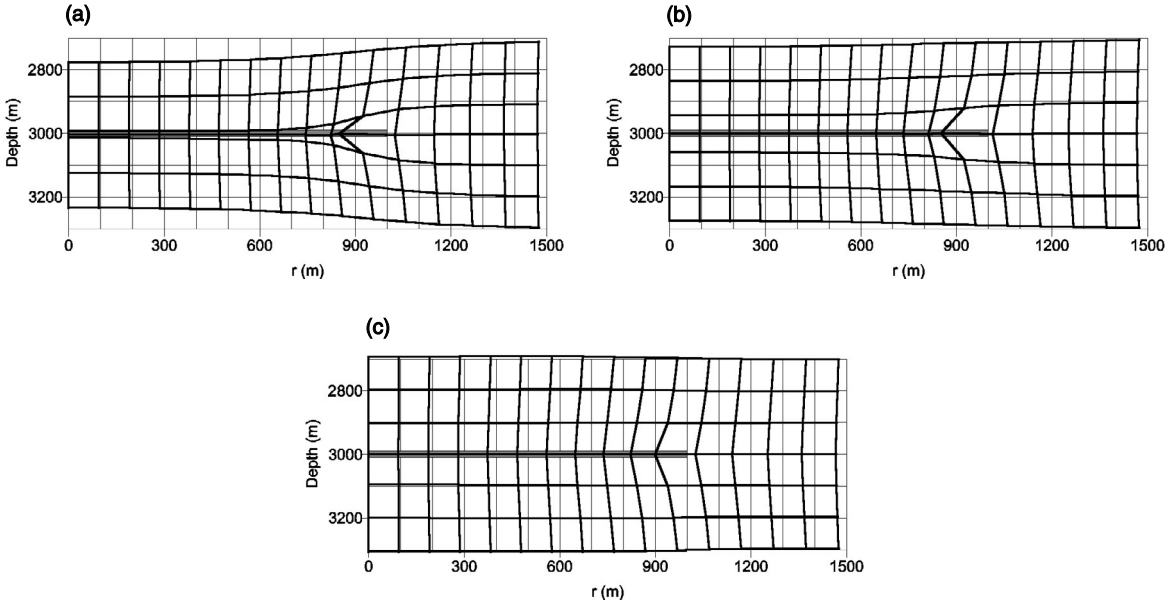

Fig. 9. Detail of the deformed medium around the reservoir for: (a) $C = 1$; (b) $C = 0.5$; (c) $C = 0.1$. The exaggeration for horizontal and vertical displacements is 10 000.

3.3. Three-dimensional elliptic reservoir

Geometry of real fields is usually more complex than that of a disk. Based on the results shown in the previous sections, we may expect a field shape other than the disk-shaped one to influence significantly the parametric analysis discussed above.

To study the importance of the shape of the depleted volume on the movement of land surface a reservoir with an elliptical horizontal cross-section is simulated. The burial depth is $h = 3000$ m, with $s = 20$ m, and $v = 0.25$. The ellipsis axes are equal to 10 000 and 2000 m with an aspect ratio of 5. A unit pressure decline is prescribed within the gas/oil bearing formation. The boundary conditions are the same as for the disk-shaped reservoir. The FE mesh used to discretize the medium consists of 11 220 nodes and 60 588 tetrahedral elements.

Land settlement at the central point η_{cen} relative to the settlement occurred in the homogeneous case vs C is shown in Fig. 11a, together with a comparison with the corresponding values obtained with the disk-shaped reservoirs having a radius R equal to 1000 and 5000 m (see Fig. 11b). It can be observed that the model addressing the elliptical reservoir exhibits an intermediate behavior between the two axisymmetric ones. This result suggests that the disk-shaped reservoirs analyzed in the previous sections may provide a useful indication about the land subsidence to be expected over elliptical or nearly elliptical fields.

4. Influence of a stiff underburden

In some field situations the compressibility contrast may not be restricted to the layer which incorporates the reservoir, but can be extended also to the underlying strata. For example, a process leading to

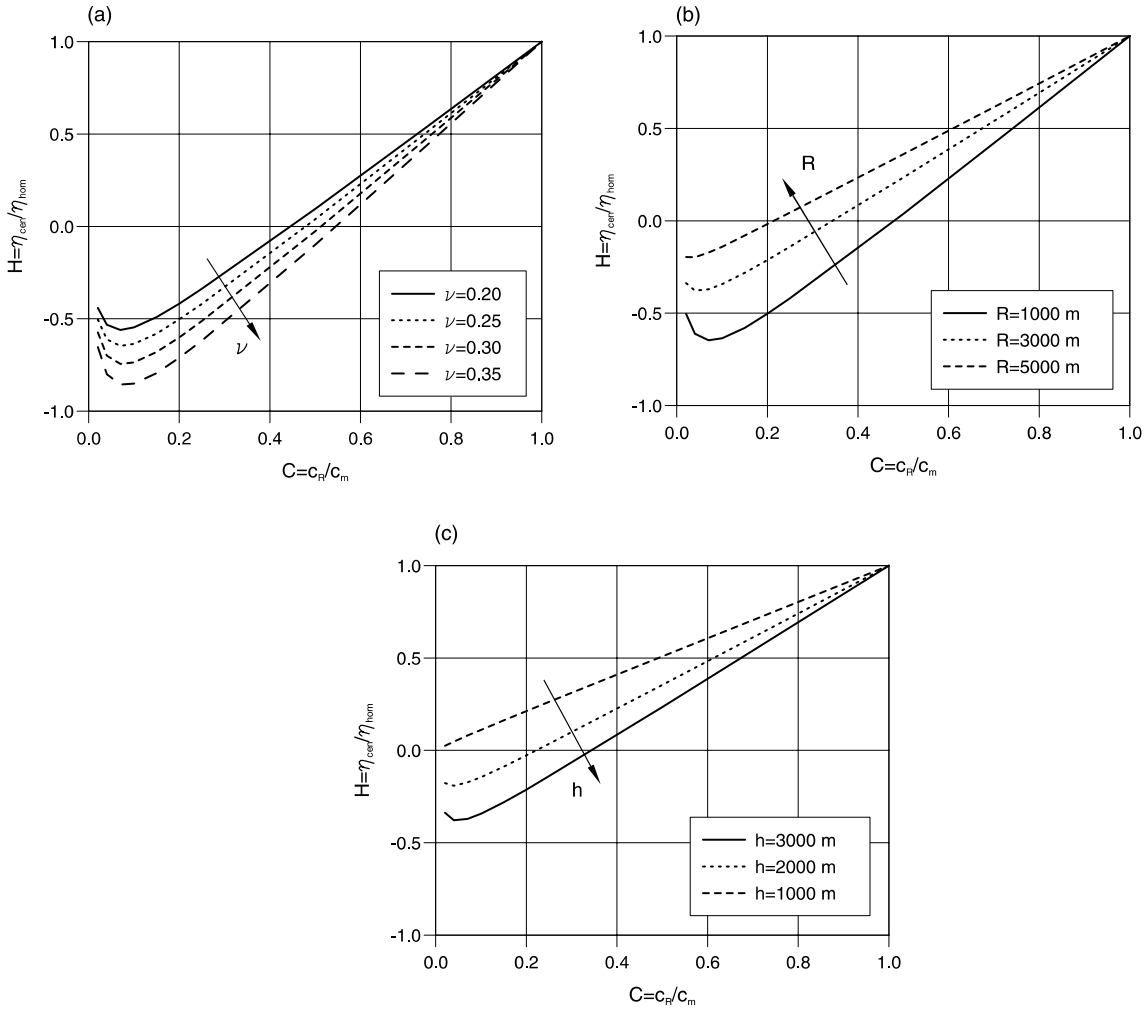

Fig. 10. H vs C for the problems with: (a) $h = 3000$ m, $R = 1000$ m, and variable v; (b) $h = 3000$ m, variable R, and $v = 0.25$; (c) variable h, $R = 3000$ m, and $v = 0.25$.

overconsolidation is the removal of overburden by erosion followed by deposition, which originates a compressibility contrast between the shallowest sediments and the underlying geological structure. We investigate the influence that an underburden stiffer than the overburden may have on the ground surface motion by assuming a smaller vertical compressibility c_u in the porous volume lying underneath the reservoir, as is schematically represented in Fig. 12a.

The same sample problem as in Section 3.1 is addressed ($h = 3000$ m, $s = 20$ m, $R = 1000$ m with a unit pore pressure decline within the reservoir) for different C, v, and c_u. In Fig. 12b H values are given for the limiting cases $c_u = c_R$ and $c_u = c_m$, and the intermediate one $c_u = 0.5(c_R + c_m)$, with $v = 0.25$ and 0.35. The results indicate that land surface deformation is strongly influenced by the stiffness of the underburden. If $c_u = c_R$, H is always larger than C, with no uplift over a compacting reservoir and no additional subsidence over a depleted expanding reservoir. Compared to the case with $c_u = c_m$, such a behavior is basically ac-

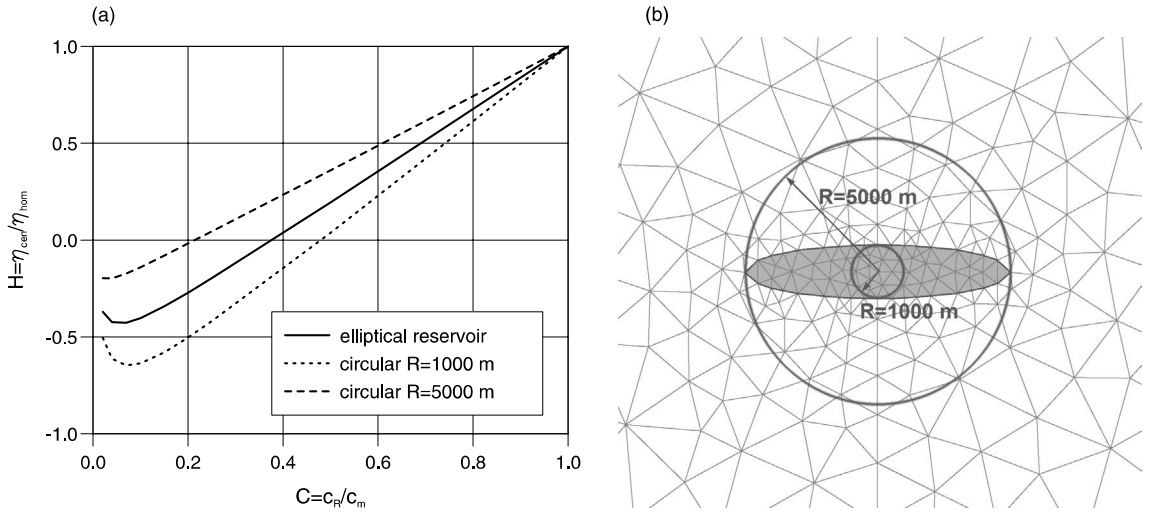

Fig. 11. (a) H vs C for the 3-D sample problem with an elliptical compacting reservoir with $h = 3000$ m, $s = 20$ m and $v = 0.25$; (b) plane view of the FE mesh with the trace of the elliptical reservoir (gray shaded) and the inscribed and circumscribed circles.

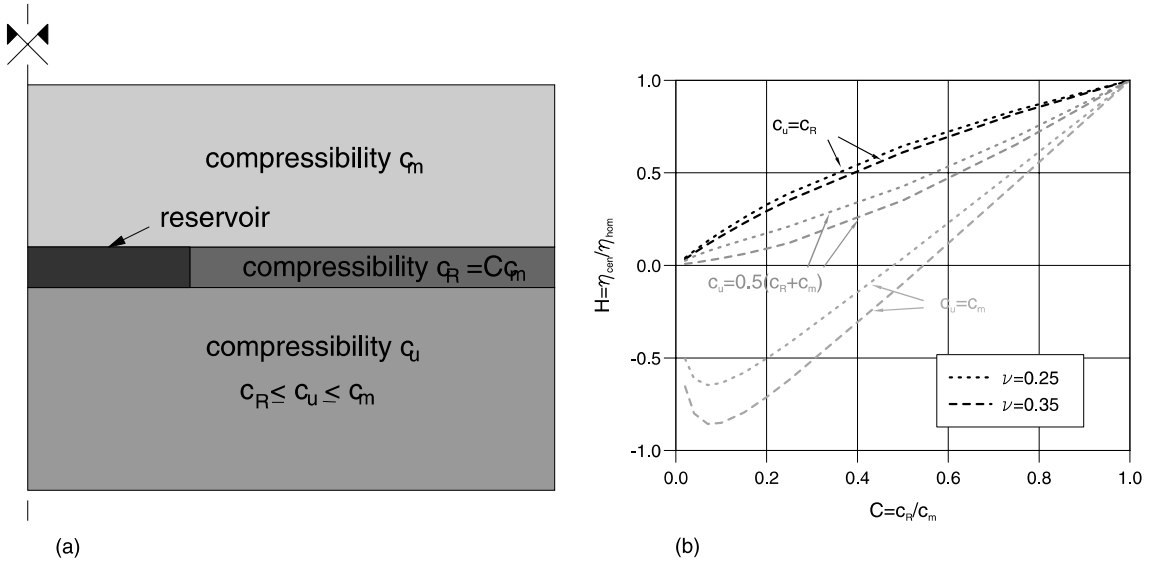

Fig. 12. (a) Schematic representation of the porous volume with a stiff underburden; (b) H vs C for the sample problem with $h = 3000$ m, $s = 20$ m, $R = 1000$ m, and various v and c_u.

counted for by the smaller upward vertical and horizontal displacements of the reservoir bottom, which no longer offset the downward motion of the reservoir top and reduce the overburden swelling, respectively. It may be noted that in the intermediate case as well no uplift occurs. However, the concavity profile changes, so that H is smaller than C. This implies that with such a configuration, i.e. $c_R < c_u < c_m$, the land settlement reduces proportionally more than the reservoir compressibility does.

5. Conclusions

Land subsidence due to the depletion of an overconsolidated gas/oil reservoir has been analyzed in a simplified linear elastic setting by the FE method using the infinite pore pressure gradient approach. Contrary the common belief the compaction of a disk-shaped reservoir stiffer than the surrounding medium may induce zero land settlement or even a surface uplift for very stiff depleted formations. This is basically due to the fact that under such conditions the reservoir mainly shrinks in the horizontal direction, thus causing a possible swelling of the overburden which emphasizes the vault effect. Similar results may be actually found in real world problems of gas/oil production from overconsolidated fields or, vice versa, additional subsidence may be experienced during recovery over exhausted formations which are known to exhibit a larger stiffness in expansion.

In particular, the following points are worth summarizing:

- compressibility ratios c_R/c_m close to 0.5, i.e. a relatively limited amount of overconsolidation, may be enough to cancel the transference of compaction to land surface over the field center depending on the value of h, R and v;
- the compaction of stiffer fields ($c_R/c_m < 0.5$) can induce an uplift that may be as much as 80% of land subsidence expected in the homogeneous problem (for $c_R/c_m \simeq 0.1$);
- the location where the largest land subsidence occurs migrates from the center of the field toward or even past the reservoir outline;
- the magnitude of uplift is basically related to the geometrical features (burial depth h and radius R) of the field, and to porous medium Poisson ratio v. In particular the overburden swelling, which is responsible for the much reduced subsidence or the uplift, is enhanced by larger h/R, i.e. deep and areally limited reservoirs, and by a larger v, which emphasizes the effect of the horizontal shrinkage on the vertical deformation;
- by distinction, uplift disappears and land subsidence becomes almost proportional to c_R/c_m, as intuition would suggest, for areally large and shallow reservoirs;
- 3-D overconsolidated fields with an elliptical horizontal cross-section exhibit an intermediate behavior between the smaller and the larger disk-shaped fields which comprise the ellipsis, so the axisymmetric results can provide some indications also for realistic 3-D reservoirs of elliptical or nearly elliptical shape;
- land surface motion is much influenced by the underburden mechanical properties and for stiff underlying formations uplift may disappear.

Acknowledgements

This study has been partially funded by the Italian MURST Project "Metodologie Innovative per il Monitoraggio, la Gestione ed il Controllo Quali-quantitativo delle Acque Sotterranee" (New Technologies for the Qualitative and Quantitative Monitoring, Management and Control of Groundwater Systems).

References

Baù, D., Gambolati, G., Teatini, P., 1999. Residual land subsidence over depleted gas fields in the Northern Adriatic Basin. Environ. Engng. Geosci. V (4), 389–405.

Baù, D., Ferronato, M., Gambolati, G., Teatini, P., 2001. Land subsidence spreading factor of the Northern Adriatic gas fields, Italy. Int. J. Geomech., in press.

Bertoni, W., Bratti, C., Carbognin, L., Cesi, C., Chierici, G.L., Dossena, G., Guerricchio, A., La Monica, U., La Tegola, A., Succetti, A., 2000. Analysis of subsidence in the Crotone area along the Ionian coast of Calabria, Italy. In: Carbognin, L., Gambolati, G., Johnson, A.I. (Eds.), Proceedings of the Sixth International Symposium on Land Subsidence, vol. 1. Ravenna, Italy, pp. 155–166.

Bévillon, D., Boutéca, M.J., Longuemare, P., 2000. Contribution of the coupled hydromechanical theory in the estimate of reservoir production. SPE 65175, Presented at the 2000 SPE European Petroleum Conference, Paris.

Biot, M.A., 1941. General theory of three-dimensional consolidation. J. Appl. Phys. 12 (2), 155–164.

Colazas, X.C., Strehle, R.W., 1995. Subsidence in the Wilmington Oil Field, Long Beach, California, USA. In: Chilingarian, G.V., Donaldson, E.C., Yen, T.F. (Eds.), Subsidence due to Fluid Withdrawal. Developments in Petroleum Science, vol. 41. Elsevier, Amsterdam, pp. 285–335.

Finol, A.S., Sancevic, Z.A., 1995. Subsidence in Venezuela. In: Chilingarian, G.V., Donaldson, E.C., Yen, T.F. (Eds.), Subsidence due to Fluid Withdrawal. Developments in Petroleum Science, vol. 41. Elsevier, Amsterdam, pp. 337–372.

Gambolati, G., 1972. A three-dimensional model to compute land subsidence. Bullet. Int. Ass. Hydrolog. Sci. 17, 219–226.

Gambolati, G., Ricceri, G., Bertoni, W., Brighenti, G., Vuillermin, E., 1991. Mathematical simulation of the subsidence of Ravenna. Water Resour. Res. 27 (11), 2899–2918.

Gambolati, G., Teatini, P., Bertoni, W., 1998. Numerical prediction of land subsidence over Dosso degli Angeli Gas Field, Ravenna, Italy. In: Borchers, J. (Ed.), Land Subsidence – Current Research and Case Studies, Proc. J. F. Poland Symp. on Land Subsidence, Sacramento, CA, October 1995, Star Publishing, Belmont, California, pp. 229–238.

Gambolati, G., Ferronato, M., Teatini, P., Deidda, R., Lecca, G., 2001. Finite element analysis of land subsidence above depleted reservoirs with the pore pressure gradient and the total stress formulations. Int. J. Numer. Anal. Meth. Geomech. 25 (4), 307–327.

Geertsma, J., 1966. Problems of rock mechanics in petroleum production engineering. In: Proc. 1st Cong. Int. Soc. Rock Mechan. Lisbon, pp. 585–594.

Geertsma, J., 1973a. A basic theory of subsidence due to reservoir compaction: the homogeneous case. Verhandelingen Kon. Ned. Geol. Mijnbouwk. Gen. 28, 43–62.

Geertsma, J., 1973b. Land subsidence above compacting oil and gas reservoirs. J. Pet. Technol. 25, 734–744.

Geertsma, J., van Opstal, G., 1973. A numerical technique for predicting subsidence above compacting reservoirs, based on the nucleus of strain concept. Verhandelingen Kon. Ned. Geol. Mijnbouwk. Gen. 28, 63–78.

Hermansen, H., Landa, G.H., Sylte, J.E., Thomas, L.K., 2000. Experiences after 10 years of waterflooding the Ekofisk Field, Norway. J. Pet. Sci. Engng. 26, 11–18.

Palozzo, W., Cassiani, G., Brighenti, G., Zoccatelli, C., 2000. Three-dimensional simulation of subsidence due to the gas production in the Barbara Field and comparison with field data. In: Carbognin, L., Gambolati, G., Johnson, A.I. (Eds.), Proceedings of the Sixth International Symposium on Land Subsidence, vol. 2. Ravenna, Italy, pp. 397–408.

Sagaseta, C., 1987. Analysis of undrained soil deformation due to ground loss. Géotechnique 37, 301–320.

Teatini, P., Gambolati, G., Tomasi, L., Putti, M., 1998. Simulation of land subsidence due to gas production at Ravenna coastline. In: Gambolati, G. (Ed.), CENAS, Coastline Evolution of the Upper Adriatic Sea due to Sea Level Rise and Natural and Anthropogenic Land Subsidence, Water Science and Technology Library, vol. 28. Kluwer Academic Publishers, Norwell, MA., pp. 135–152.

Teatini, P., Baù, D., Gambolati, G., 2000. Water-gas dynamics and coastal land subsidence over Chioggia Mare Field, Northern Adriatic Sea. Hydrogeo. J. 8 (5), 462–479.

Terzaghi, K., Peck, R.B., 1967. Soil Mechanics in Engineering Practice, second ed. Wiley, New York.

Verruijt, A., 2000. Subsidence of an elastic half space by extraction of oil or gas. Private Communication, Technology University of Delft.

Zaman, M.M., Abdulraheem, A., Roegiers, J.C., 1995. Reservoir compaction and surface subsidence in the North Sea Ekofisk Field. In: Chilingarian, G.V., Donaldson, E.C., Yen, T.F. (Eds.), Subsidence due to Fluid Withdrawal. Developments in Petroleum Science, vol. 41. Elsevier, Amsterdam, pp. 373–423.

Zienkiewicz, O.C., Taylor, R.L., 1989. The Finite Element Method, fourth ed. McGraw Hill, London.